ACCOUNTS of chemical research

Article

pubs.acs.org/accounts

Computational Insights into the Central Role of Nonbonding Interactions in Modern Covalent Organocatalysis

Published as part of the Accounts of Chemical Research special issue "Computational Catalysis for Organic Synthesis".

Daniel M. Walden,[†] O. Maduka Ogba,[†] Ryne C. Johnston,[‡] and Paul Ha-Yeon Cheong*[,†]

[†]Department of Chemistry, Oregon State University, 153 Gilbert Hall, Corvallis, Oregon 97331, United States

[‡]UT/ORNL Center for Molecular Biophysics, Biosciences Division, Oak Ridge National Laboratory, 1 Bethel Valley Road, Oak Ridge, Tennessee 37830, United States

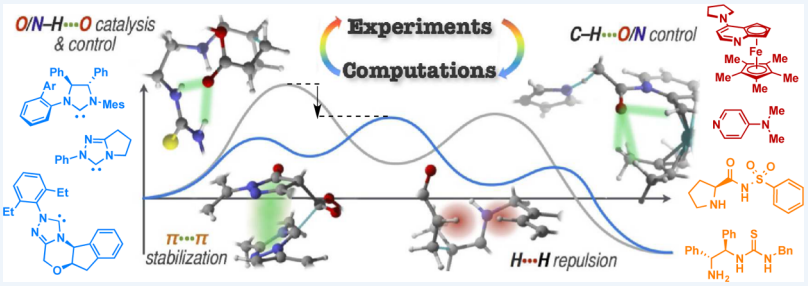

CONSPECTUS: The flexibility, complexity, and size of contemporary organocatalytic transformations pose interesting and powerful opportunities to computational and experimental chemists alike. In this Account, we disclose our recent computational investigations of three branches of organocatalysis in which nonbonding interactions, such as C−H···O/N interactions, play a crucial role in the organization of transition states, catalysis, and selectivity.

We begin with two examples of N-heterocyclic carbene (NHC) catalysis, both collaborations with the Scheidt laboratory at Northwestern. In the first example, we discuss the discovery of an unusual diverging mechanism in a catalytic kinetic resolution of a dynamic racemate that depends on the stereochemistry of the product being formed. Specifically, the major product is formed through a concerted asynchronous [2 + 2] aldol-lactonization, while the minor products come from a stepwise spiro-lactonization pathway. Stereoselectivity and catalysis are the results of electrophilic activation from C−H···O interactions between the catalyst and the substrate and conjugative stabilization of the electrophile. In the second example, we show how knowledge and understanding of the computed transition states led to the development of a more enantioselective NHC catalyst for the butyrolactonization of acyl phosphonates. The identification of mutually exclusive C−H···O interactions in the computed major and minor TSs directly resulted in structural hypotheses that would lead to targeted destabilization of the minor TS, leading to enhanced stereoinduction. Synthesis and evaluation of the newly designed NHC catalyst validated our hypotheses.

Next, we discuss two works related to Lewis base catalysis involving 4-dimethylaminopyridine (DMAP) and its derivatives. In the first, we discuss our collaboration with the Smith laboratory at St Andrews, in which we discovered the origins of the regioselectivity in carboxyl transfer reactions. We disclose how different Lewis base catalysts (NHC or DMAP) can lead to different regiomeric products as a result of differing magnitudes of aromatic and C−H···O interactions present in the respective transition states. In the second example, we discuss the mechanism and origins of the stereoselectivity of a reaction catalyzed by a planar-chiral 4-(pyrrolidino)pyridine derivative, namely, the coupling of ketenes with cyanopyrrole. We discovered that the chiral base mechanism is operative, in contrast to the originally proposed Brønsted acid mechanism. The selectivity is determined by the ease with which the major and minor TSs can realize strong stabilizing C−H···N interactions between the pyrrole cyano group and the catalyst. These interactions induce increased catalyst distortion in the minor TS, thereby leading to enantioselectivity.

Finally, we discuss our computations related to amine-based organocatalysis in collaboration with the Carter laboratory at Oregon State. We probed the mechanism and stereoselectivity of a bifunctional amine thiourea-catalyzed Michael reaction. Our computations led to the design of an improved catalyst. However, synthesis and tests revealed that this catalyst was prone to degradation to side products that also catalyze the reaction, ultimately reducing the observed enantioselectivity. Lastly, we discuss our study of the mechanism and stereoselectivity of a proline sulfonamide-catalyzed Robinson annulation, in which we discovered that the enantioselectivity is controlled by the first Michael step but the diastereoselectivity is controlled by the following Mannich step.

1. INTRODUCTION

Advances in affordable computing technologies and new quantum-mechanical theories have expanded the reach of quantum

Received: April 30, 2016
Published: June 6, 2016

DOI: 10.1021/acs.accounts.6b00204
Acc. Chem. Res. 2016, 49, 1279−1291

mechanics from simplified models with many structural approximations and truncations to large, realistic systems with considerable conformational flexibility and structural complexity. Theory remains a powerful tool in the chemist's arsenal, and demonstrations of its power in the generation of chemical hypotheses that govern selectivities, reactivities, and mechanisms abound in the literature,[1] as revealed in no small part by the collection of articles presented in this special issue of *Accounts of Chemical Research*.

The increasingly complex and multifunctional nature of contemporary organocatalytic transformations complicate the generation of hypotheses, as List observed nearly a decade ago, "Often there is little knowledge of a given reaction mechanism and the exact mode of activation is unknown."[2] Our laboratory focuses on the application of state-of-the-art electronic structure methods to real-world catalytic reactions. We perform mechanistic analyses and create transition state (TS) models to explain selectivity in contemporary synthetic transformations through experimental collaboration[3] or in important classes of reactions that have gone unstudied by theory because of their complexity.

In covalent catalysis, the substrate is recognized and bound as an activated catalyst−substrate complex, profoundly altering the substrate frontier molecular orbitals to unlock or lower previously inaccessible reactivities. Catalyst electron donation facilitates HOMO activation to generate a nucleophilic complex. Conversely, LUMO-activating catalysts increase the electrophilicity of the substrate by functioning as an electron-withdrawing group. Moreover, many catalysts can demonstrate both types of activation (i.e., bifunctional). We and others are discovering the rich and unusual variety of activation modes of nonbonding interactions that are present in modern covalent organocatalyses. Of primary importance to our studies have been "nonclassical" hydrogen bonds (e.g., C−H···O),[4,5] in which a polarized C−H bond is in close proximity to a base, often with a developing negative charge, such as a carbonyl undergoing nucleophilic attack. Activated C_{sp^3}−H groups adjacent to partial or full positive charges and most $C_{sp^2/sp}$ groups stabilize both ground-state[6] and TS structures.[4] We also underscore the importance of C−H···N interactions,[7] which operate in catalysis similarly to their oxygen counterparts.

In the following studies, we highlight the fundamental role of these and other interactions in a diverse array of organocatalytic reactions. While C−H···O/N interactions are not always the only stabilizing interactions in a TS, they play pivotal roles in contributing to the overall catalysis or selectivity by stabilizing developing charges and/or providing electrophilic activation. It is our hope in this Account to illustrate the challenge involved in identifying hypotheses and theories governing the reactivity and selectivities of modern organocatalytic transformations when multiple nonbonding interactions are at play simultaneously. Furthermore, we demonstrate the ability of theory to drive catalyst design.

2. COMPUTATIONAL METHODS

When studying reactions using theory, the proper choice of a computational method is of utmost importance. A great number of factors contribute to the choice, and thus, the process is nontrivial. Alignment of computational data with experimental observations is necessary for reliable theoretical analyses and computational predictions.[8] Many of the methods used in the following sections were the results of extensive benchmarking to locate a combination of methods, basis sets, and solvation models that best matches key experimental parameters.

In order to calculate reaction stereo- and regioselectivity, we compute reaction coordinates, including selectivity- and rate-determining TSs and all pertinent ground-state intermediates leading to each product. The free energy span[9] can be estimated using transition state theory, specifically by applying Eyring's equation,[10] given experimental parameters of temperature (T), reaction time (t), and yield (Y) together with the universal gas constant (R), Planck's constant (h), and Boltzmann's constant (k_B):

$$\Delta G^{\ddagger} = -RT \ln\left[\frac{h \ln\left(\frac{100}{100 - Y}\right)}{tTk_B}\right]$$

We quantify catalyst control of the product distribution (e.g., the diastereomeric ratio, dr) by computing the relative rates, i.e., the difference of the relative free energies ($\Delta\Delta G^{\ddagger}$), of the product-determining TSs. The product ratios and the relative rates of their formation are derived from the following expression:

$$k_{rel} = e^{\Delta\Delta G^{\ddagger}/RT}$$

The differences in energy between the major and minor TSs, in addition to all of the relevant conformers, can be quite small (<2 kcal/mol). Accurate computational methods are therefore necessary to capture the inter- and intramolecular forces relevant to the chemistry.

Two common hybrid functionals are employed for the systems reported in this Account: (1) The popular B3LYP[11] hybrid generalized gradient approximation (GGA) functional owes its enduring ubiquity in applied computational studies of organic systems to its speed, robust description of electrostatic interactions, and efficient error cancellation. A longstanding deficiency of hybrid functionals is the treatment of dispersion interactions. To correct for this in B3LYP-optimized structures (except in section 3.2), we performed single-point energy refinements using Grimme's spin-component-scaled second-order Møller−Plesset (SCS-MP2) perturbation theory[12] coupled with triple- and quadruple-ζ-quality Ahlrich basis sets[13] extrapolated to the complete basis set limit (def2-∞). This combination of theories was used to model the reactions disclosed in sections 5.1 and 5.2. (2) Systems disclosed in sections 3.1, 4.1, and 5.2 were modeled with the hybrid meta-GGA functional M06-2X, which can account for dispersion interactions.[14] We further refined the energies using single-point refinements with larger Pople basis sets[15] including additional polarization and diffuse functions.[16] Implicit solvation corrections were applied using either the polarized continuum model (PCM)[17] (sections 3.1, 4.1, 4.2, and 5.2) or SMD[18] (section 5.1).

3. N-HETEROCYCLIC CARBENE CATALYSIS

N-Heterocyclic carbene (NHC) catalysts feature a central *N*-alkyl- or *N*-aryl-substituted azolium ring, which generates a stable singlet carbene upon deprotonation of the interstitial methine at C2. Nucleophilic carbene catalysts induce unique and tunable reactivities in carbonyl compounds by virtue of the push−pull electronics of the conjugated azolium ring in the Breslow-like intermediates.[19] We have used quantum-mechanical computations to study the mechanisms and stereomechanics of three different NHC-catalyzed transformations: β-lactonization of a dynamically racemizing substrate (section 3.1), γ-lactonization of acyl

DOI: 10.1021/acs.accounts.6b00204
Acc. Chem. Res. 2016, 49, 1279−1291

phosphonates (section 3.2), and regiodivergent and catalyst-specific carboxyl transfer (section 4.1).

3.1. Catalytic Kinetic Resolution of Dynamically Racemizing β-Keto Esters

Methods furnishing enantioenriched products from racemic starting materials are appealing techniques in organic synthesis because of their cost and step efficiency. Of particular importance is dynamic kinetic resolution (DKR), in which a substrate undergoing rapid racemization reacts with a catalyst, stereospecifically and irreversibly transforming a single substrate enantiomer into product.[20] In view of the theoretical yield of 100%, DKR provides an atom-economical synthetic route to a great number of valuable bioactive compounds.[21] β-Keto esters are primed for DKR reactions because of the lability of the α-proton, allowing interconversion between the keto ester and the achiral enol. The asymmetric synthesis of substituted β-lactones can be achieved through NHC-catalyzed lactonization of β-keto esters.[22] We investigated the mechanism and origins of stereoselectivity in this reaction through a joint experimental and computational effort with the Scheidt group at Northwestern (Scheme 1).[23]

Scheme 1. NHC-Catalyzed Kinetic Resolution of a Dynamic Racemate; Synthesis of a β-Lactone from β-Keto Ester

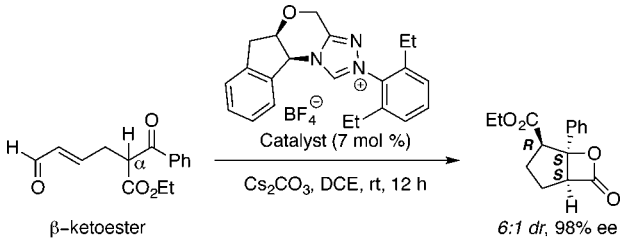

3.1.1. Dynamic Kinetic Resolution. The NHC-catalyzed DKR process relies on the facile epimerization of the β-keto ester starting material under the basic conditions needed for carbene generation.[24] The NHC forms a key NHC−enol/enolate intermediate with the terminal aldehyde, which then undergoes stereospecific intramolecular aldol addition to one enantiomer of the β-keto ester, selectively trapping the *R* substrate over the *S* epimer through a low-energy lactonization TS ($k_R > k_S$) (Scheme 2). Overall, the reaction selectively produces an enantioenriched lactone from four possible diastereomeric products with good dr (6:1) and high enantioselectivity (98% ee).

Scheme 2. Racemization of the NHC−Enol/Enolate Complex Allows Stereospecific Lactonization

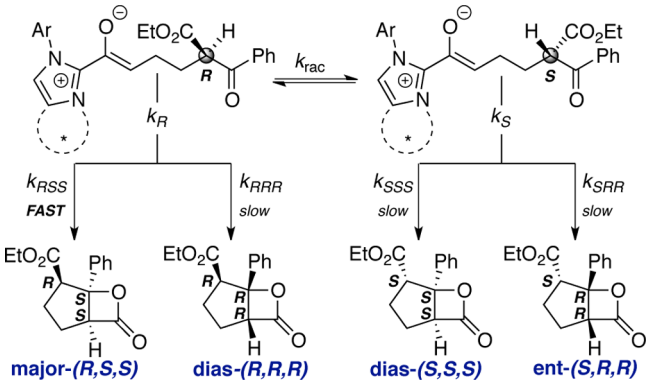

Scheme 3. Computed Catalytic Cycle Showing Three Possible Divergent Mechanisms for Lactone Formation

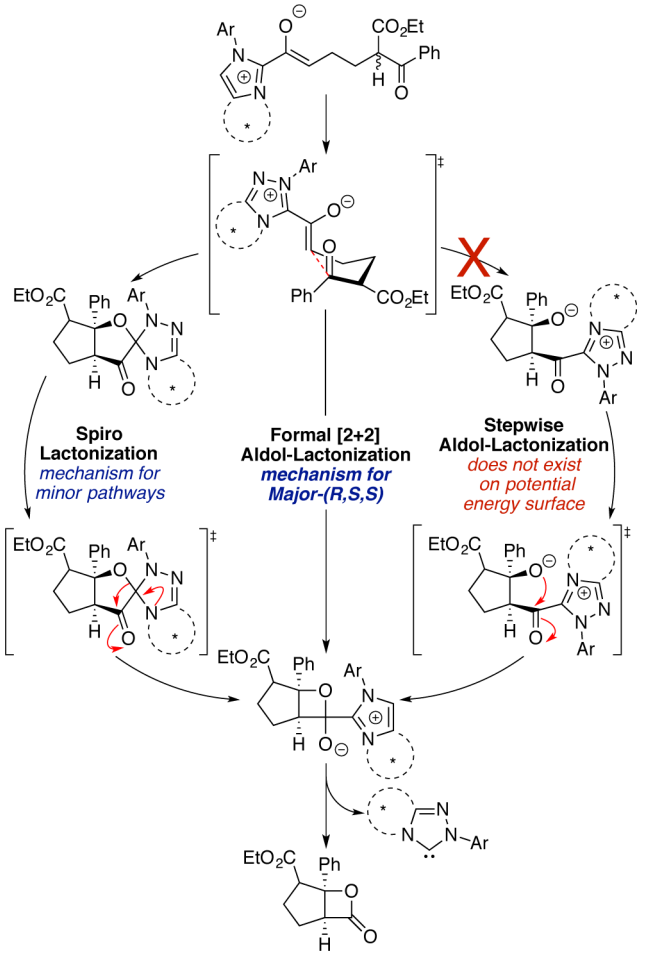

3.1.2. Catalytic Cycle. The zwitterionic NHC−enol/enolate intermediate (Scheme 3, top) is in rapid equilibrium with its α-epimer. Our computations indicated that aldol-lactonization occurs via the enolate and not the enol.[25] At this point, three mechanisms were postulated, all of which lead to the β-lactone product. We began with the stepwise aldol-lactonization mechanism previously proposed by Romo[26] and echoed more recently by Paddon-Row and Lupton,[27] featuring aldol C−C bond formation and subsequent C−O ring closure (Scheme 3, right). All computational efforts to locate the alkoxide intermediate led to its collapse on either the carbonyl or the azolium, indicating that this intermediate does not exist on the potential energy surface (PES) for this reaction. Instead, we found an unusual divergence into two mechanisms, depending on which C−C diastereoisomer is formed. The **major-(*R*,*S*,*S*)** lactone is formed from a concerted formal [2 + 2] mechanism (Scheme 3, middle), leading directly to the tetrahedral intermediate.[28] All of the minor stereoisomers undergo a stepwise spiro-lactonization mechanism (Scheme 3, left), in which a spiro-aminal ether intermediate forms following alkoxide attack of the NHC. Ring contraction furnishes the NHC−lactone tetrahedral intermediate. Product release regenerates the NHC.

3.1.3. Transition State Stabilization. Three important factors control the selectivity and catalysis (Figure 1): (1) C−H···O stabilization of the developing alkoxide by catalyst C−H donors, (2) conjugative stabilization of the electrophilic carbonyl by the adjacent aryl π system, and (3) van der Waals

DOI: 10.1021/acs.accounts.6b00204
Acc. Chem. Res. 2016, 49, 1279−1291

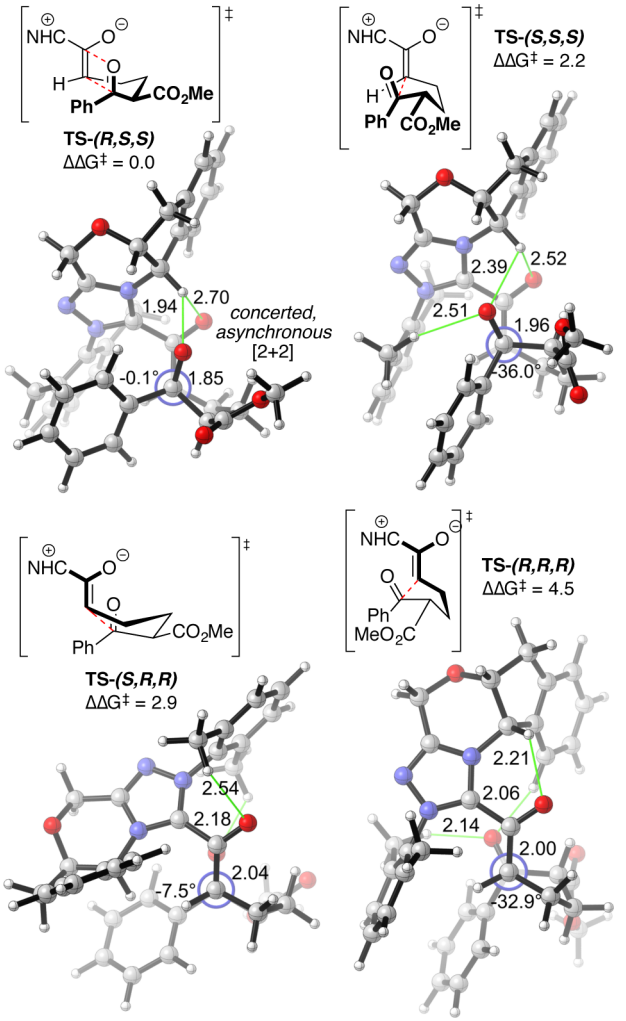

Figure 1. Rate and stereodetermining aldol-lactonization TSs. All of the structures are oriented looking down the forming C−C bond. Green lines indicate C−H···O stabilization. Dihedral angles are given as a measure of planarity of the electrophilic carbonyl and the adjacent Ph group.[29]

attraction between the substrate aryl and the catalyst. Of the four diastereomeric TSs, major **TS-(*R*,*S*,*S*)** shows the highest degree of conjugative stabilization (−0.1°). In addition, it experiences the strongest C−H···O nonbonding stabilization (1.94 Å) from the acidic NHC pyranyl C−H, which is polarized by the ortho, cationic NHC.

3.1.4. Origins of Stereoselectivity. The diastereoselectivity results from the difference in energy between major **TS-(*R*,*S*,*S*)** and **TS-(*S*,*S*,*S*)**, with $\Delta\Delta G^{\ddagger}$ = 2.2 kcal/mol, in reasonable agreement with experiments (1.1 kcal/mol). The C−H···O distance in the minor diastereomer **TS-(*S*,*S*,*S*)** is longer (2.39 Å) and weaker. Moreover, this TS suffers from decreased conjugative stabilization of the electrophilic carbonyl (−36.0° vs −0.1°). The enantioselectivity results from the difference in energy between major **TS-(*R*,*S*,*S*)** and **TS-(*S*,*R*,*R*)** and is in excellent agreement with experiment (2.9 vs 2.9 kcal/mol). The C−H···O interaction in the minor enantiomer **TS-(*S*,*R*,*R*)** involves a much weaker donor C−H from the catalyst aryl substituent (2.54 Å). These findings illustrate the subtle competitions between C−H donors and conjugative stabilizations that ultimately control the selectivity and reactivity in this dynamic kinetic process.

3.2. Computationally-Guided Optimization of NHC-Catalyzed Butyrolactonization from Acyl Phosphonates

Theory has the potential to drive catalyst design. A second NHC-mediated reaction studied in our laboratory was a collaborative theoretical and experimental investigation of the synthesis of γ-butyrolactones from acyl phosphonates, again with the Scheidt group (Scheme 4).[30] Acyl phosphonates are valuable substrates

Scheme 4. Optimized Conditions for the NHC-Catalyzed Synthesis of γ-Butyrolactones

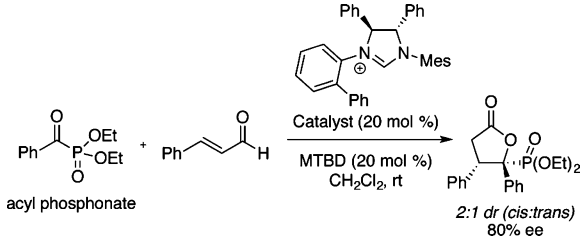

in a number of metal-catalyzed synthetic methods, including Mukaiyama−Michael reactions,[31] Friedel−Crafts indole alkylations,[32] and hetero-Diels−Alder reactions.[33] In the present reaction, a biaryl-saturated imidazolium-derived organocatalyst was found to furnish γ-butyrolactones from acyl phosphonates with high enantioselectivity (80% ee) and good dr (cis:trans = 2:1). During the optimization process, a host of imidazoliums were explored but were found to give suboptimal yields and enantioselectivities. Our goal in this collaboration was to use quantum mechanics to computationally design a modified biaryl-saturated imidazolium catalyst to improve the enantioselectivity.

3.2.1. Catalytic Cycle. The proposed mechanism for this transformation (Scheme 5) begins with the formation of the

Scheme 5. Catalytic Cycle for the NHC-Catalyzed Synthesis of γ-Butyrolactones

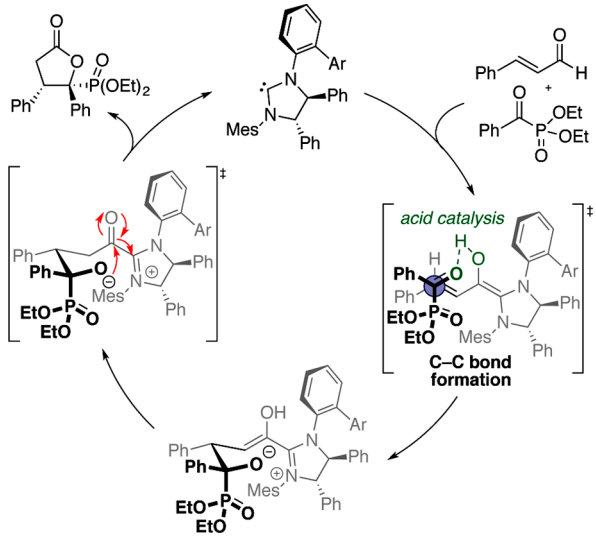

Breslow intermediate. The Breslow enol provides significant structural preorganization and activation through a hydrogen bond with the ketone of the approaching acyl phosphonate in the homoaldol addition. Tautomerization of the nascent enol to the acyl azolium intermediate followed by C−O ring closure affords the lactone product and releases the catalyst.

DOI: 10.1021/acs.accounts.6b00204
Acc. Chem. Res. 2016, 49, 1279−1291

3.2.2. Transition State Stabilization. We computed the stereodetermining C−C bond-forming homoaldol TSs for the formation of the major and minor products in order to elucidate the interactions responsible for the enantioselectivity (Figure 2).

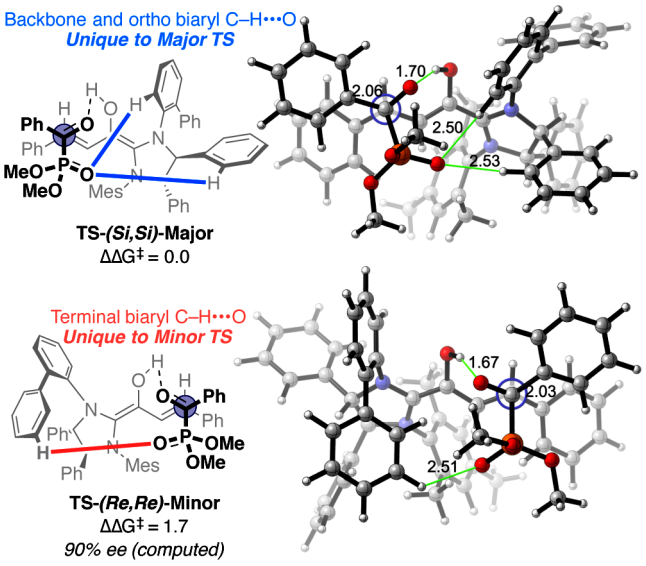

Figure 2. Computed stereodetermining TSs using the parent catalyst. The *Re*/*Si* notation indicates the prochirality of the homoenol face followed by the acyl phosphonate face. Et groups were modeled as Me groups for efficiency. The thick blue lines indicate stabilizing electrostatic interactions found only in **TS-(*Si,Si*)-Major**, while the thick pink line indicates a C−H···O interaction found only in **TS-(*Re,Re*)-Minor**. These same interactions are shown as thin green lines in the 3D structures.[29]

In all of the TSs, concerted proton transfer occurs from the Breslow enol OH to the electrophilic carbonyl. This acid catalysis is concomitant with nucleophilic attack and is a crucial component contributing to the overall catalysis of the reaction.

3.2.3. Origins of Stereoselectivity. **TS-(*Si,Si*)-Major** is 1.7 kcal/mol lower in energy than **TS-(*Re,Re*)-Minor**, corresponding to an enantioselectivity of 90% ee, which is slightly overestimated but in decent agreement with the experimental value of 80% ee. We identified unique nonbonding interactions found in the major and minor TSs. In **TS-(*Si,Si*)-Major**, two unique C−H···O interactions engage the P═O oxygen atom (blue lines, Figure 2): (1) an ortho C−H from one of the NHC backbone Ph groups and (2) an ortho C−H from the *N*-biaryl of the catalyst. In **TS-(*Re,Re*)-Minor**, approach from the opposite face of the homoenol precludes any C−H···O interactions from the backbone Ph groups. Instead, a meta C−H from the terminal Ph of the *N*-biaryl system engages in a C−H···O interaction with the acyl phosphonate P═O (pink line, Figure 2).

3.2.4. Catalyst Optimization. With the knowledge of these mutually exclusive interactions in hand, we could then propose a modification of the catalyst seeking higher enantioselectivity (Figure 3). In order to induce increased selectivity, either the energy of the major TS must be decreased or the energy of the minor TS must be increased. Since only **TS-(*Re,Re*)-Minor** enjoys stabilizing electrostatic interactions at the meta position of the terminal biphenyl, elimination of these C−H···O interactions through methylation was proposed to increase the energy of the minor pathway while having a negligible effect on the major pathway. The computed homoaldol TSs with the redesigned NHC predicted significantly increased selectivity of 99% ee. Experiments corroborated this increase, showing 84% ee with the

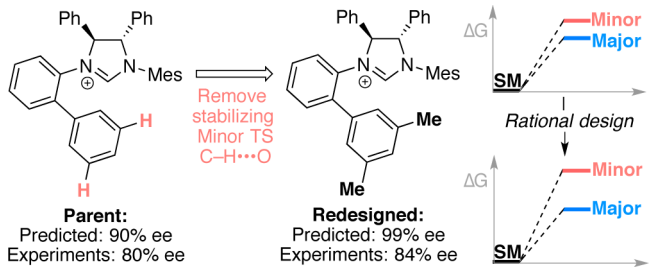

Figure 3. Computationally guided catalyst redesign to selectively destabilize the minor TS over the major TS, leading to improved selectivity.

redesigned methylated catalyst. Additional runs with bulkier Et groups instead of Me yielded an even higher selectivity of 88% ee. Ultimately, determination of the nonbonding C−H···O interactions that control the selectivity using computations was critical to understanding the stereoselectivity and realizing the rational design of a new NHC catalyst.

4. DMAP CATALYSIS

Much like NHC catalysts, 4-dimethylaminopyridine (DMAP) catalysts are potent Lewis base catalysts. In section 4.1 we describe the origins of the regiocontrol in NHC- and DMAP-catalyzed pyrazolyl carboxyl transfer. Section 4.2 describes our studies of asymmetric protonation chemistry involving a planar-chiral 4-(pyrrolidino)pyridine derivative.

4.1. Catalyst-Controlled and Regiodivergent Carboxyl Transfer

In collaboration with the Smith group at St Andrews, we investigated the origins of catalyst-controlled regioselectivity of *O*- to *C*- or *N*-carboxyl transfer of pyrazolyl carbonates. NHCs (e.g. triazolinylidenes) predominantly give the *C*-carboxylate product, and DMAP gives the *N*-carboxylate product (Scheme 6). We provided

Scheme 6. Optimized Synthetic Conditions for Catalyst-Controlled Regiodivergent Carboxyl Transfer

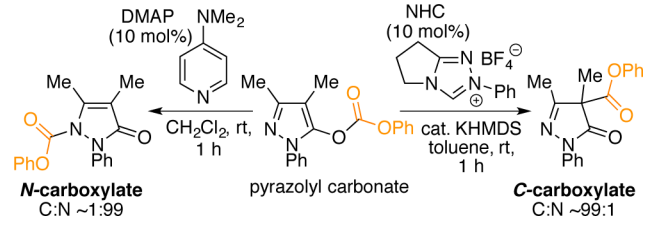

mechanistic understanding and revealed the interactions responsible for the observed regioselectivity by applying quantum-mechanical computations on a representative model system (using CO_2Me instead of CO_2Ph).[34]

This class of rearrangements, initially described by Steglich and Höfle,[35] has seen widespread synthetic application. A number of groups have demonstrated the ability of achiral and chiral DMAP derivatives to yield all-carbon quaternary stereocenters through this transformation. Both Fu[36] and Vedejs[37] developed chiral DMAP catalysts for enantioselective *O*- to *C*-carboxyl transfer of related carbonates. Smith has also shown that NHCs are able to catalyze *O*- to *C*-carboxyl transfer.[38]

4.1.1. Catalytic Cycle. We have computed all of the intermediates and transition states for both the *O*- to *C*- and *O*- to *N*-carboxyl transfer catalytic cycles for both NHC and DMAP (Scheme 7). Initial catalyst attack forms an ion pair between the

DOI: 10.1021/acs.accounts.6b00204
Acc. Chem. Res. 2016, 49, 1279−1291

Scheme 7. Computed Catalytic Cycles for *O*- to *C*- or *N*-Carboxyl Transfer

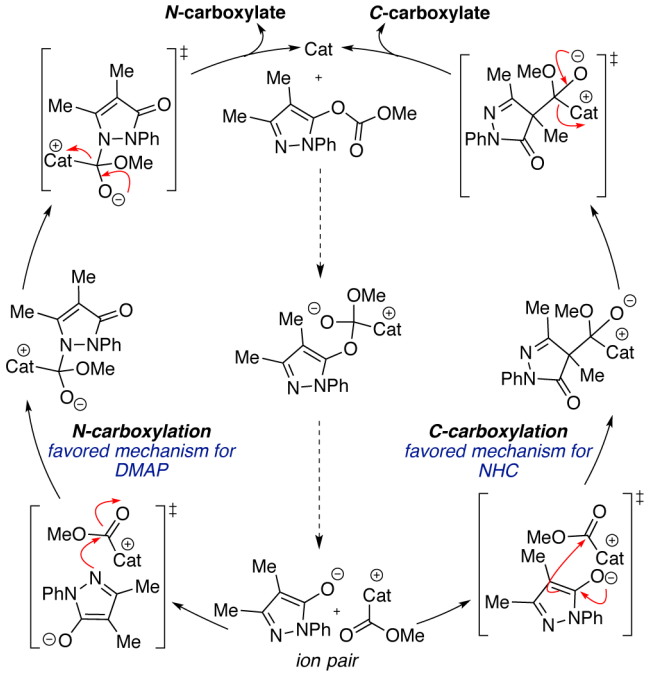

acylated catalyst and the enolate species in a stepwise fashion. The formation of this complex was also invoked in a recent computational study of the Steglich rearrangement of oxindole derivatives by Suga[39] and is supported by X-ray crystal structures.[40] Regiodivergence occurs through preferential attack on the acylated catalyst by the enolate at C4 or N1. The carboxyl transfer process is stepwise for all of the pathways except for DMAP-catalyzed C-carboxylation.[41]

4.1.2. Origins of Regioselectivity. Figure 4 shows the computed regiodetermining TSs for the DMAP and NHC catalyses. In the case of DMAP, the regiodetermining TSs involve enolate attack of the acylated catalyst for both pathways. In **TS-DMAP-*N*-Major** ($\Delta G^{\ddagger}$ = 19.2 kcal/mol), there is a large degree of stabilizing overlap between the positively charged pyridine ring and the negatively charged enolate during C−N bond formation. **TS-DMAP-*C*** ($\Delta G^{\ddagger}$ = 26.6 kcal/mol) does not benefit from significant overlap of the zwitterionic π systems, resulting in a higher-energy TS.

In the case of NHC, the highest-energy regiodetermining TSs were computed as the catalyst release step of the mechanism. In **TS-NHC-*C*-Major** ($\Delta G^{\ddagger}$ = 12.7 kcal/mol), significant overlap between the catalyst and the enolate is evident. In addition, there are two key stabilizing C−H···O interactions: (1) an ortho Ph C−H from the catalyst *N*-Ar substituent donates to the transferring carboxyl C═O (2.29 Å), and (2) an activated C−H ortho to the positively charged catalyst azolium ring donates to the substrate enolate oxygen atom (2.27 Å). **TS-NHC-*N*** ($\Delta G^{\ddagger}$ = 16.2 kcal/mol) is higher in energy as a result of the weaker interaction between the methoxy oxygen of the transferred carboxyl and the activated C−H ortho to the catalyst azolium ring (2.47 Å).

4.2. Coupling of Pyrrole to Ketenes Using Planar-Chiral PPY*

4.2.1. Planar-Chiral DMAP Catalysis. Fu's planar-chiral 4-(pyrrolidino)pyridine-derived catalyst PPY* represents a well-known class of DMAP nucleophilic catalysts[42] used in a number of asymmetric transformations involving ketenes.[43] We focused

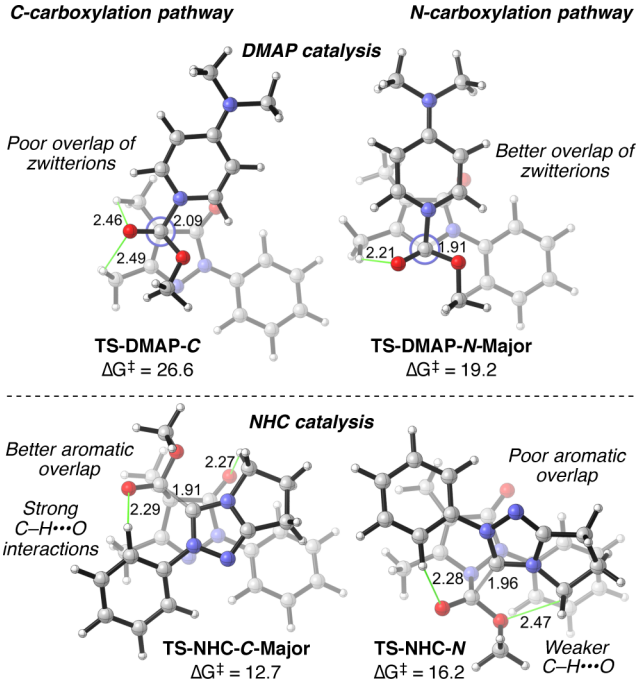

Figure 4. Computed regioselective TSs for DMAP- and NHC-catalyzed carboxyl transfer. CO_2Ph was modeled as CO_2Me for computational efficiency. Stabilizing C−H···O interactions are shown as green lines. Gray lines represent forming/breaking bonds.[29]

our efforts on understanding the origins of the catalysis and stereocontrol in the enantioselective coupling of ketenes with pyrroles furnishing *N*-acylpyrroles (Scheme 8).[44,45] At the time

Scheme 8. PPY*-Catalyzed Enantioselective Coupling of Ketenes with Pyrroles

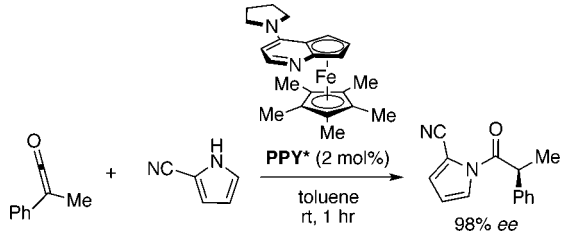

of publication, the exact mechanism and stereomechanics in this entire series of reactions were unknown. Leveraging computed and experimental kinetic isotope effects (KIEs), we deciphered the operative mechanism and discovered that C−H···O/N interactions are critical for both TS stabilization and enantioselectivity in this reaction.

4.2.2. Proposed Mechanisms. A chiral Brønsted acid pathway was originally proposed on the basis of ^{1}H NMR observations of the pyrrole−PPY* Brønsted acid resting-state complex (Figure 5a, right).[44] It was thought that protonated PPY* acts as a chiral proton source to enantioselectively protonate the pyrrole ketene enolate, leading to product formation and regenerating the catalyst. We computed all of the intermediates and TSs along this pathway and found that the rate-determining step is **TS Pyrrole-Enolate Formation** (Figure 5b), with $\Delta G^{\ddagger}$ = 23.4 kcal/mol, which is slightly above the estimated experimental barrier of 22 kcal/mol.[10]

A second mechanism for the transformation can be envisioned in which PPY* directly attacks the ketene to form a chiral enolate base (Figure 5a, left). Subsequent enantioselective protonation

DOI: 10.1021/acs.accounts.6b00204
Acc. Chem. Res. 2016, 49, 1279−1291

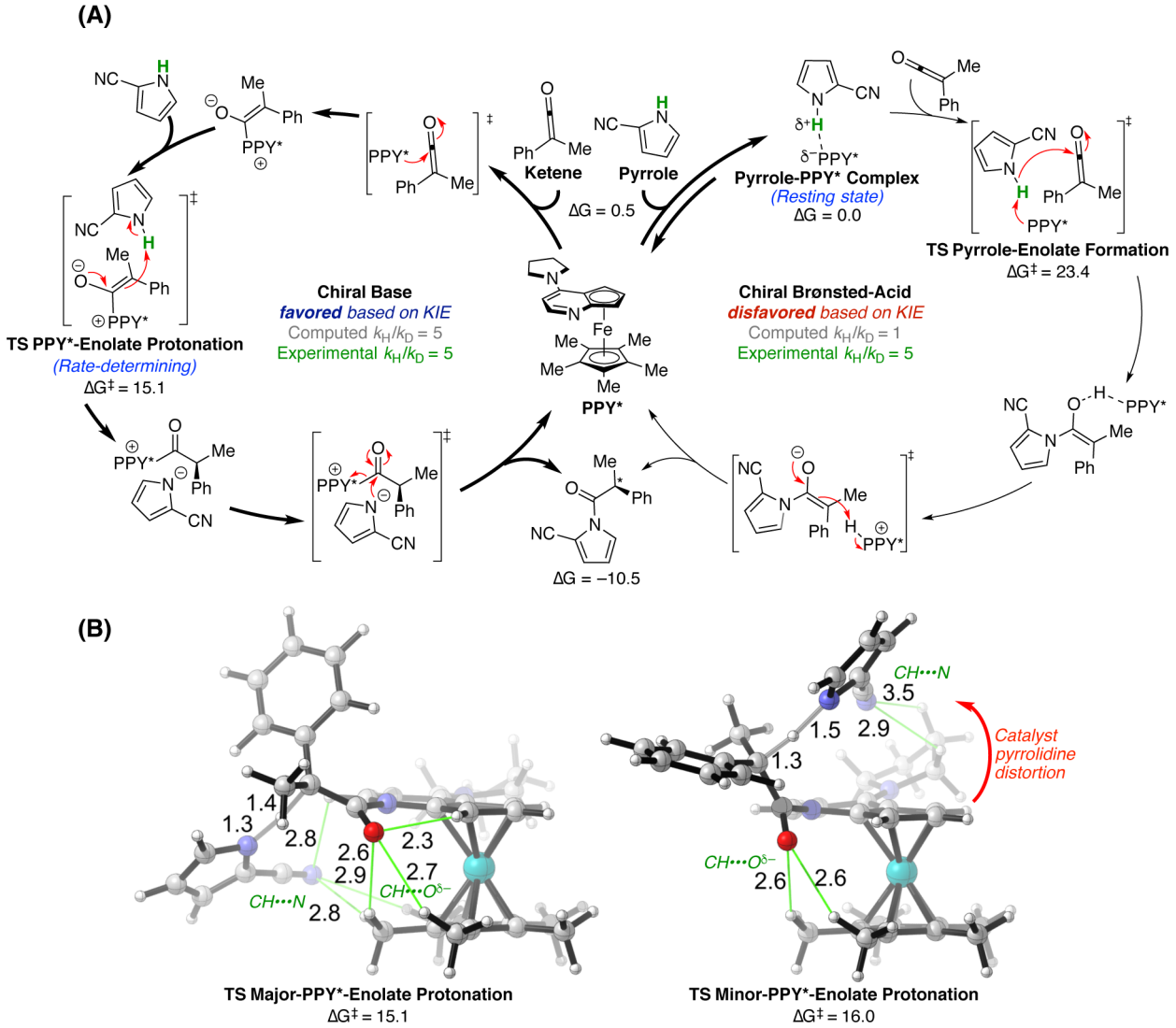

Figure 5. (a) Computed catalytic cycle. (b) Transition structures **TS Major-PPY*-Enolate Protonation** and **TS Minor-PPY*-Enolate Protonation** for the reaction in Scheme 8. CH···$O^{\delta-}$ and CH···N interactions stabilize both **Major** and **Minor**. The selectivity arises from catalyst distortion to achieve C−H···N interactions in **Minor**.[29]

of the enolate by pyrrole is rate- and stereodetermining (**TS PPY*-Enolate Protonation**, $\Delta G^{\ddagger}$ = 15.1 kcal/mol; Figure 5b). Attack at N by the pyrrole on the acylated PPY* then releases the product and regenerates the catalyst. A comparison of the computed barriers for the two mechanisms favors the chiral base pathway over the chiral Brønsted acid pathway by ∼8 kcal/mol.

4.2.3. KIE as a Key Litmus Test for Distinguishing between Proposed Mechanisms. The original experimental report by Fu reported a competition isotope experiment. With N-deuterated cyanopyrrole, a significant primary k_H/k_D of 5 was observed (eq 1). We computed the KIEs of the rate-determining

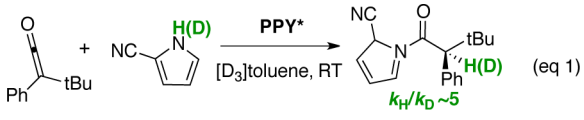

(eq 1)

TSs for both the chiral base and chiral Brønsted acid mechanisms (**TS PPY*-Enolate-Protonation** and **TS Pyrrole-Enolate-Formation**, respectively; Figure 5).[46] The result for the chiral base mechanism was consistent with experiments (**TS PPY*-Enolate-Protonation**: k_H/k_D = 5), whereas the experimental KIE was decisively inconsistent with that for the chiral Brønsted acid mechanism (**TS Pyrrole-Enolate Formation**: k_H/k_D = 1). The combined KIE experiments and computational results as well as the computed energetics suggest that although the resting-state complex is consistent with the chiral Brønsted acid pathway, the chiral base pathway is operative in this reaction (Figure 6).

4.2.4. Transition State Stabilization and Origins of Selectivity. With knowledge of the productive pathway, we probed the nonbonding interactions stabilizing the key rate- and stereodetermining enolate protonation transition state (Figure 5b). In both **TS Major-PPY*-Enolate Protonation** and **TS Minor-PPY*-Enolate Protonation**, the enolate oxygen is sandwiched between the rings of PPY* through stabilizing C−H···O interactions worth ∼3−4 kcal/mol according to the model systems. The incoming pyrrole anion cyano C−N also enjoys stabilizing C−H···N interactions with the catalyst. However, the selectivity is ultimately determined by the ability of the catalyst to stabilize the incoming pyrrole anion through the C−H···N interactions. In **Major** (*Re* approach), the pyrrole is positioned between the rings of PPY* through C−H···N interactions

DOI: 10.1021/acs.accounts.6b00204
Acc. Chem. Res. 2016, 49, 1279−1291

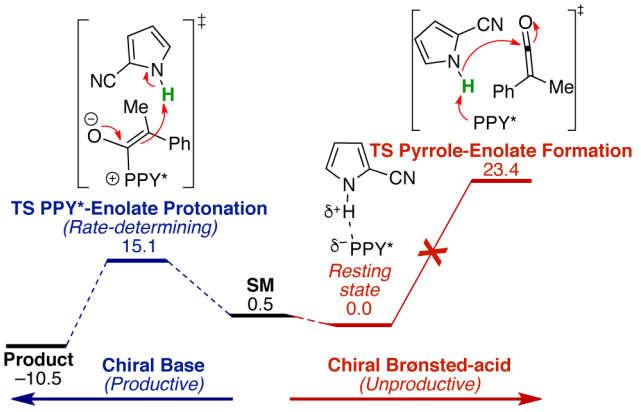

Figure 6. Curtin−Hammett kinetic scenario operative in planar-chiral DMAP (PPY*)-catalyzed coupling of pyrroles and ketenes.

requiring minimal catalyst distortion. In **Minor** (*Si* approach), the pyrrole is projected above PPY* and is stabilized through C−H···N interactions with the catalyst pyrrolidine. In contrast to **Major**, the catalyst is distorted in **Minor** in order to achieve stabilizing C−H···N interactions and is consequently higher in energy by 0.9 kcal/mol, a selectivity value consistent with experiment ($\Delta\Delta G^{\ddagger}_{expt}$ = 1.3 kcal/mol).

5. AMINE CATALYSIS

Catalysts with amine functionality typically provide reactivity through the generation of nucleophilic enamine species or electrophilic iminium ions.[47] In section 5.1, we investigate the selectivity of a bifunctional primary amine thiourea-catalyzed cyclization. Section 5.2 provides our detailed description of a proline sulfonamide-catalyzed Robinson annulation.

5.1. Bifunctional Primary Amine Thiourea-Catalyzed Construction of All-Carbon Stereocenters

Efficient routes to install all-carbon quaternary stereocenters remain one of the holy grails in synthetic chemistry.[48] Pfau and d'Angelo provided an appealing stereoselective method to synthesize 2,2-disubstituted cycloalkanones bearing an all-carbon quaternary stereocenter using stoichiometric α-methyl benzylamine.[49] Building on this pioneering work, the Carter laboratory at Oregon State rendered the original stoichiometric reaction catalytic using a thiourea-based[50] dual-activation strategy (Scheme 9).[51] In

Scheme 9. Amine Thiourea-Catalyzed Construction of Stereogenic α,α-Disubstituted Cycloalkanones

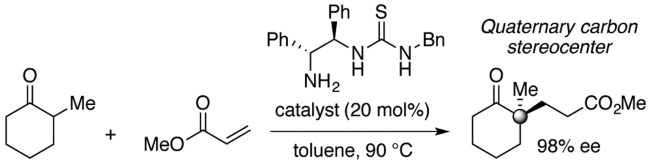

collaboration, we used computations to provide insights into the mechanism and stereoselectivity.[52] We also used this information in an effort to design a catalyst with improved selectivity.

5.1.1. Catalytic Cycle. The catalyst condenses with its primary amine on the cycloalkanone to furnish the imine (Scheme 10). In agreement with the experimentally observed 8:1 equilibrium favoring the imine, computations showed that the imine is energetically lower by 1.6 kcal/mol (9:1). The small concentration of enamine formed is consumed by rate- and stereodetermining Michael addition **TS-Michael-(*R,R*)-Major** ($\Delta G^{\ddagger}$ = 24.7 kcal/mol).

Scheme 10. Computed Catalytic Cycle for the Amine Thiourea-Catalyzed Synthesis of Cycloalkanones

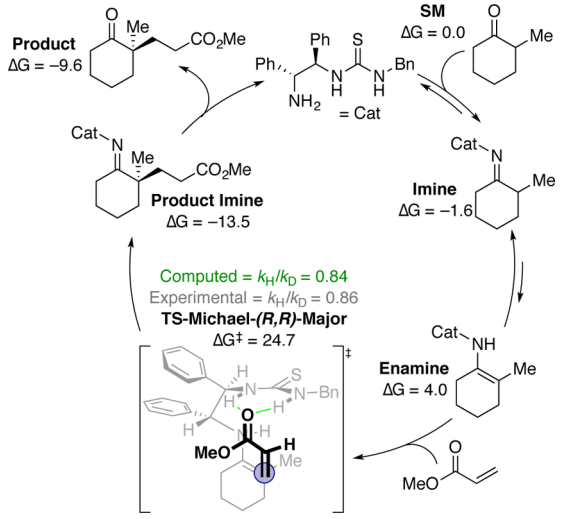

A secondary KIE experiment with olefin-deuterated methyl acrylate as the electrophile was performed (eq 2). The computed k_H/k_D of

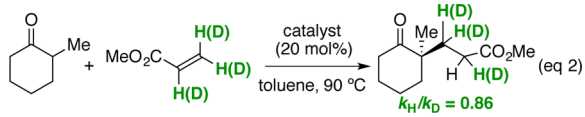

0.84 was in excellent agreement with experiments (k_H/k_D = 0.86), corroborating the C−C bond-forming Michael TS as rate-determining.[53] Facile proton transfer and hydrolysis release the product and regenerate the catalyst.

5.1.2. Transition State Stabilization. In this reaction, three main factors contribute to TS stabilization (Figure 7):[54,55] (1) nucleophilic activation of the donor cycloalkanone through formation of an enamine, (2) electrophilic activation of the acrylate C═O through hydrogen bonding to the thiourea, and (3) electrostatic stabilization of the developing negative charge on the electrophile through proximity to the developing positive charge of the catalyst iminium.

5.1.3. Origins of Stereoselectivity. Stereoinduction is provided by the chiral scaffold bridging the two activating components. **TS-Michael-(*S,S*)-Minor** ($\Delta\Delta G^{\ddagger}$ = 5.1 kcal/mol) places the electrophile exo to the enamine ring and forces the catalyst α-phenyl group to be in close repulsive contact (2.00 Å) with the incoming electrophile. This destabilizing interaction is stronger than the attractive C−H···O interaction between the catalyst β-phenyl group and the electrophile C═O. On the basis of these findings, the Carter group synthesized the des-β-phenyl catalyst in hopes of improving the enantioselectivity. However, this new catalyst decomposed under the reaction conditions to form products including benzylamine, which can itself catalyze the reaction racemically, ultimately leading to reduced enantioselectivity.

5.2. Proline Sulfonamide-Catalyzed Robinson Annulation

Over four decades ago, Hajos and Parrish[56] described a proline-catalyzed intramolecular aldol reaction, one of the first examples of modern organocatalysis. Proline organocatalysis has since become a comprehensive and expanding field[57] that has been well-studied both experimentally[58] and theoretically.[1,59] In this final section, we describe our computational investigation of the mechanism and stereomechanics of a proline sulfonamide-catalyzed synthesis

DOI: 10.1021/acs.accounts.6b00204
Acc. Chem. Res. 2016, 49, 1279−1291

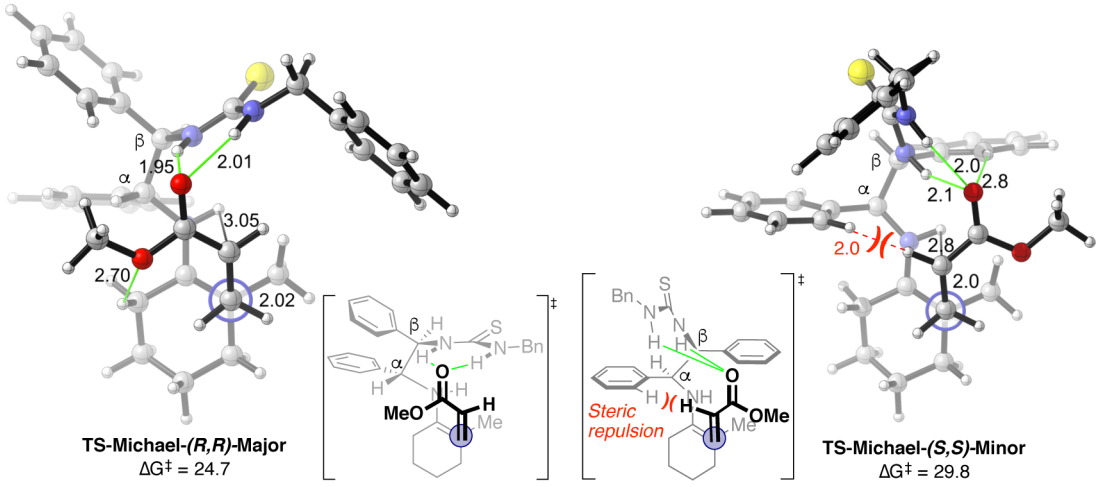

Figure 7. Computed rate- and stereodetermining TSs for the amine thiourea-catalyzed synthesis of cycloalkanones.[29]

of enantio- and diastereoenriched cyclohexenones containing γ-quaternary and δ-tertiary all-carbon stereocenters (Scheme 11) in collaboration with the Carter group at Oregon State.[60]

Scheme 11. Dual Amino-Catalyzed Robinson Annulation

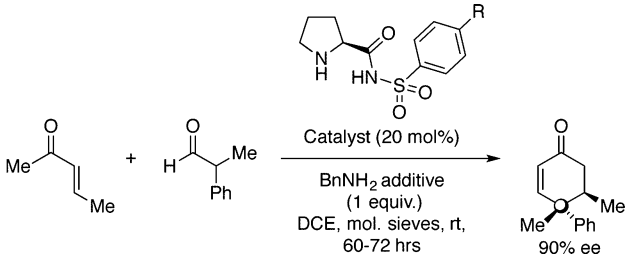

5.2.1. Catalytic Cycle. We studied six mechanisms that could account for the formation of the cyclohexenone product on a representative model system (SO_2Ar in the catalyst was computed as SO_2Me and $BnNH_2$ as $MeNH_2$). All of the computational evidence led to the conclusion that the Michael–Mannich mechanism shown in Scheme 12 is operative in this transformation, and thus, it is the focus in this Account.

The resting state of this reaction is the imine formed from the aldehyde and amine additive (Scheme 12, top). Complete consumption of the aldehyde and concomitant formation of the imine are observed by ^{1}H NMR spectroscopy when benzylamine and substituted aldehydes are premixed. This imine is in dynamic equilibrium with the aldenamine. Addition of the proline sulfonamide catalyst to the ketone forms the catalyst iminium. Michael addition between the catalyst iminium and the reactive aldenamine followed by tautomerization leads to the pre-Mannich enamine. Mannich annulation followed by hydrolysis produces the cyclohexenone product and releases the proline sulfonamide catalyst.

5.2.2. Duumvirate Stereocontrol. The Michael addition transition state is rate-determining for the formation of both the major and minor enantiomeric cyclohexenone products, while the Mannich annulation is rate-limiting for the diastereomeric product (Figure 8). Therefore, both transition states must be considered for a complete understanding of the stereoselectivity in this reaction. We call this duumvirate[61] stereocontrol.

5.2.3. Transition State Stabilization. As seen in other proline-catalyzed asymmetric reactions, the key Michael and

Scheme 12. Catalytic Cycle for the Process Shown in Scheme 11

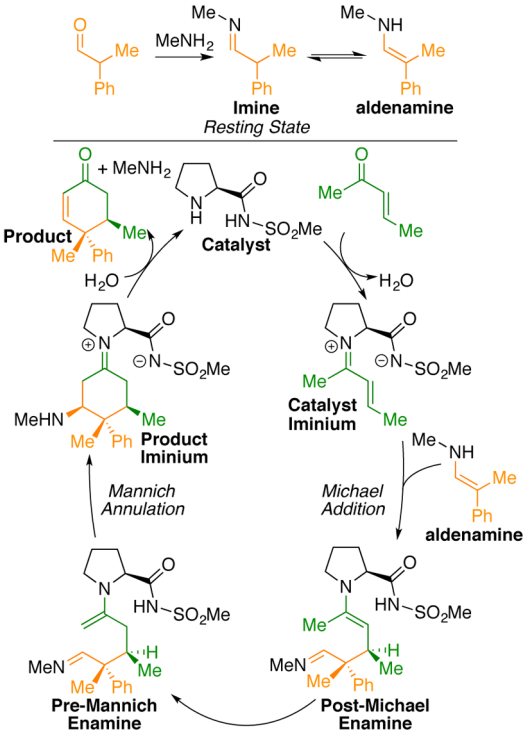

Mannich transition structures are stabilized by hydrogen bonds with the proline acidic moiety,[57] in this case the sulfonamide. Hydrogen bonding between the approaching aldenamine and the sulfonamide is a necessary element of both the stereocontrol and catalysis, as evidenced by poor catalysis by proline itself and other tetrazole catalysts.

5.2.4. Origins of Stereoselectivity. The enantioselectivity in this reaction is governed by the syn/anti catalyst iminium preference. We found an unusual preference for the *syn*-iminium over the *anti*-iminium in the Michael addition. In the absence of other intervening effects, syn transition states in organocatalytic reactions are typically disfavored because the catalyst iminium/enamine must distort from planarity to accommodate the close proximity of the approaching substrate to the hydrogen-bonding catalyst side chain.[59,1] However, in this particular reaction, the vinylogous electrophilic iminium activation further removes the

DOI: 10.1021/acs.accounts.6b00204
Acc. Chem. Res. 2016, 49, 1279–1291

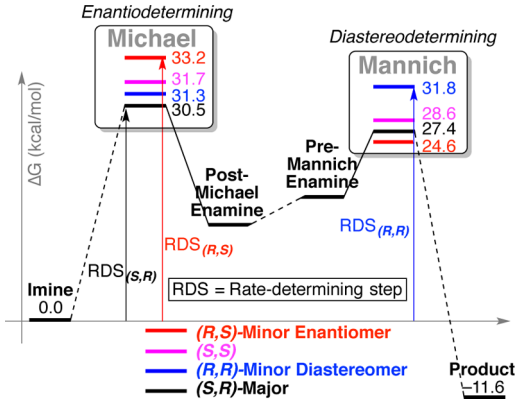

Figure 8. Duumvirate stereocontrol is operative: the Michael addition controls the enantioselectivity and the Mannich annulation controls the diastereoselectivity.

C−C bond-forming center from the catalyst side chain, changing the optimal hydrogen-bonding distance. Consequently, geometric distortions in the catalyst iminium necessitate hydrogen bonding to a more distal aldenamine, consistently destabilizing the *anti*-iminium Michael TSs (Figure 9). Specifically, the catalyst in the **Minor-*Ent*-*anti*-*si*-(*R*,*S*)** Michael TS has a distorted planarity

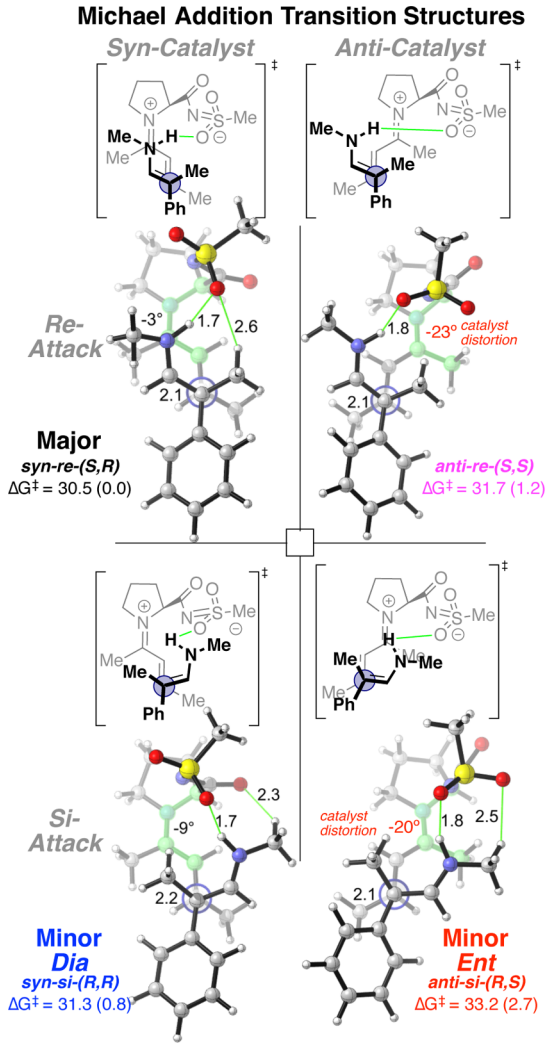

Figure 9. Michael addition TSs.[29]

of −20° versus −3° in **Major-*syn*-*re*-(*S*,*R*)** (dihedral angles highlighted in green) and is consequently higher in energy by 2.7 kcal/mol.

The diastereoselectivity is decided by the Mannich step (Figure 10). The minor diastereomeric product is the (*R*,*R*) product.

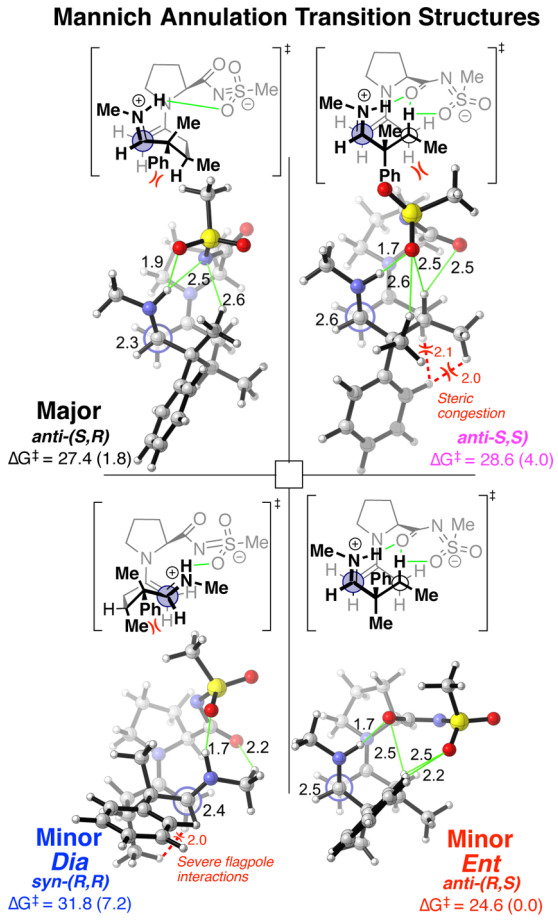

Figure 10. Mannich annulation TSs.[29]

The Mannich TS leading to this product (**Minor-*Dia*-*syn*-(*R*,*R*)**) is the most disfavored over the other diastereomers. Two features destabilize this TS: (1) as discussed earlier, the *syn*-enamine is disfavored in the Mannich annulation,[59] and (2) severe flagpole steric interactions caused by an axial methyl group in the boatlike conformation of the forming six-membered ring further raise the barrier.

6. CONCLUSION

In this Account, we have described the application of the tools of computational chemistry to six modern organocatalytic reactions in order to elucidate the operative mechanism and reveal the nonbonding interactions responsible for transition state stabilization and selectivity. Through these studies, we have observed the importance of C−H···O/N and other nonbonding interactions in providing catalysis and selectivity. The complex modes of activation and product differentiation described here suggest that more complex interplays between nonbonding interactions underpin many modern synthetic transformations. Through synergistic efforts with synthetic collaborators, we have also shown how these computationally derived hypotheses can lead to the development of new catalysts and improved processes. We have only begun to explore the full power of what theory can unfold, and we continue to

DOI: 10.1021/acs.accounts.6b00204
Acc. Chem. Res. 2016, 49, 1279−1291

build on these experiences and discoveries to tackle increasingly complex and powerful transformations using theory.

AUTHOR INFORMATION

Corresponding Author

*E-mail: paulc@science.oregonstate.edu.

Notes

The authors declare no competing financial interest.

Biographies

Daniel M. Walden received his B.S. in chemistry from Humboldt State University, Arcata, California, in 2013. He is currently a third-year Ph.D. student.

O. Maduka Ogba is a 2016 Robbins Postdoctoral Fellow, Pomona College. He received his B.S. in computer science with a minor in chemistry from Trinity University, San Antonio, Texas, in 2011 and his Ph.D. in chemistry from Oregon State University in 2016.

Ryne C. Johnston is a UT/ORNL Center for Molecular Biophysics Postdoctoral Fellow, Oak Ridge National Laboratory. He received his B.S. from Henderson State University, Arkadelphia, Arkansas, in 2010 and his Ph.D. from Oregon State University in 2015.

Paul Ha-Yeon Cheong is the Bert and Emelyn Christensen Professor at Oregon State University. He received his A.B. from Bowdoin College, Brunswick, Maine, in 2001 and his Ph.D. from UCLA in 2007.

ACKNOWLEDGMENTS

P.H.-Y.C. is the Bert and Emelyn Christensen Professor and gratefully acknowledges financial support from the Stone Family of OSU. Financial support from the National Science Foundation (NSF) (CHE-1352663) is acknowledged. D.M.W., O.M.O., R.C.J., and P.H.-Y.C. also acknowledge computing infrastructure in part provided by the NSF Phase-2 CCI, Center for Sustainable Materials Chemistry (CHE-1102637). We are grateful to Professors Karl A. Scheidt (Northwestern), Andrew D. Smith (St Andrews), and Rich G. Carter (Oregon State) for experimental collaborations.

ABBREVIATIONS

DFT, density functional theory; TS, transition structure; SM, starting material; PES, potential energy surface; DKR, dynamic kinetic resolution; KIE, kinetic isotope effect; RDS, rate-determining step

REFERENCES

(1) Cheong, P. H.-Y.; Legault, C. Y.; Um, J. M.; Çelebi-Ölçüm, N.; Houk, K. N. Quantum mechanical investigations of organocatalysis: Mechanisms, reactivities, and selectivities. *Chem. Rev.* **2011**, *111*, 5042−5137.

(2) List, B. Introduction: Organocatalysis. *Chem. Rev.* **2007**, *107*, 5413−5415.

(3) Cheng, G.-J.; Zhang, X.; Chung, L. W.; Xu, L.; Wu, Y.-D. Computational organic chemistry: Bridging theory and experiment in establishing the mechanisms of chemical reactions. *J. Am. Chem. Soc.* **2015**, *137*, 1706−1725.

(4) Johnston, R. C.; Cheong, P. H.-Y. C−H···O non-classical hydrogen bonding in the stereomechanics of organic transformations: Theory and recognition. *Org. Biomol. Chem.* **2013**, *11*, 5057−5064.

(5) (a) Mittal, N.; Lippert, K. M.; De, C. K.; Klauber, E. G.; Emge, T. J.; Schreiner, P. R.; Seidel, D. A dual-catalysis anion-binding approach to the kinetic resolution of amines: Insights into the mechanism via a combined experimental and computational study. *J. Am. Chem. Soc.* **2015**, *137*, 5748−5758. (b) Maity, P.; Pemberton, R. P.; Tantillo, D. J.; Tambar, U. K. Brønsted acid catalyzed enantioselective indole aza-Claisen rearrangement mediated by an arene CH−O interaction. *J. Am. Chem. Soc.* **2013**, *135*, 16380−16383. (c) Scheiner, S.; Grabowski, S. J.; Kar, T. Influence of hybridization and substitution on the properties of the CH···O hydrogen bond. *J. Phys. Chem. A* **2001**, *105*, 10607−10612. (d) Vargas, R.; Garza, J.; Dixon, D. A.; Hay, B. P. How strong is the C^{α}-H···O═C hydrogen bond? *J. Am. Chem. Soc.* **2000**, *122*, 4750−4755.

(6) (a) Yates, J. R.; Pham, T. N.; Pickard, C. J.; Mauri, F.; Amado, A. M.; Gil, A. M.; Brown, S. P. An investigation of weak CH···O hydrogen bonds in maltose anomers by a combination of calculation and experimental solid-state NMR spectroscopy. *J. Am. Chem. Soc.* **2005**, *127*, 10216−10220. (b) Desiraju, G. R. The C-H···O hydrogen bond in crystals: What is it? *Acc. Chem. Res.* **1991**, *24*, 290−296.

(7) Brovarets, O. O.; Yurenko, Y. P.; Hovorun, D. M. Intermolecular CH···O/N H-bonds in the biologically important pairs of natural nucleobases: a thorough quantum-chemical study. *J. Biomol. Struct. Dyn.* **2014**, *32*, 993−1022.

(8) (a) Plata, R. E.; Singleton, D. A. A case study of the mechanism of alcohol-mediated Morita Baylis-Hillman reactions. The importance of experimental observations. *J. Am. Chem. Soc.* **2015**, *137*, 3811−3826. (b) Gutierrez, O.; Strick, B. F.; Thomson, R. J.; Tantillo, D. J. Mechanism of triflimide-catalyzed [3,3]-sigmatropic rearrangements of *N*-allylhydrazones−predictions and experimental validation. *Chem. Sci.* **2013**, *4*, 3997−4003.

(9) (a) Kozuch, S.; Amatore, C.; Jutand, A.; Shaik, S. What makes for a good catalytic cycle? A theoretical study of the role of an anionic palladium(0) complex in the cross-coupling of an aryl halide with an anionic nucleophile. *Organometallics* **2005**, *24*, 2319−2330. (b) Yu, Z.-X.; Cheong, P. H.-Y.; Liu, P.; Legault, C. Y.; Wender, P. A.; Houk, K. N. Origins of differences in reactivities of alkenes, alkynes, and allenes in [Rh(CO)2Cl]2-catalyzed (5 + 2) cycloaddition reactions with vinylcyclopropanes. *J. Am. Chem. Soc.* **2008**, *130*, 2378−2379. (c) Cohen, S.; Kozuch, S.; Hazan, C.; Shaik, S. Does substrate oxidation determine the regioselectivity of cyclohexene and propene oxidation by cytochrome P450? *J. Am. Chem. Soc.* **2006**, *128*, 11028−11029.

(10) Eyring, H. The activated complex in chemical reactions. *J. Chem. Phys.* **1935**, *3*, 107−115.

(11) (a) Becke, A. D. Density-functional thermochemistry. III. The role of exactl exchange. *J. Chem. Phys.* **1993**, *98*, 5648−5652. (b) Lee, C.; Yang, W.; Parr, R. G. Development of the Colle-Salvetti correlation-energy formula into a functional of the electron density. *Phys. Rev. B: Condens. Matter Mater. Phys.* **1988**, *37*, 785−789.

(12) (a) Gerenkamp, M.; Grimme, S. Spin-component scaled second-order Møller−Plesset perturbation theory for the calculation of molecular geometries and harmonic vibrational frequencies. *Chem. Phys. Lett.* **2004**, *392*, 229−235.

(13) Weigend, F.; Ahlrichs, R. Balanced basis sets of split valence, triple zeta valence and quadruple zeta valence quality for H to Rn: Design and assessment of accuracy. *Phys. Chem. Chem. Phys.* **2005**, *7*, 3297−3305.

(14) Zhao, Y.; Truhlar, D. G. The M06 suite of density functionals for main group thermochemistry, thermochemical kinetics, noncovalent interactions, excited states, and transition elements: two new functionals and systematic testing of four M06-class functionals and 12 other functionals. *Theor. Chem. Acc.* **2008**, *120*, 215−241.

(15) Hehre, W. J.; Ditchfield, R.; Pople, J. A. Self−consistent molecular orbital methods. XII. Further extensions of Gaussian−type basis sets for use in molecular orbital studies of organic molecules. *J. Chem. Phys.* **1972**, *56*, 2257−2261.

(16) Hariharan, P. C.; Pople, J. A. The influence of polarization functions on molecular orbital hydrogenation energies. *Theor. Chim. Acta* **1973**, *28*, 213−222.

(17) Miertuš, S.; Scrocco, E.; Tomasi, J. Electrostatic interaction of a solute with a continuum. A direct utilization of AB initio molecular potentials for the prevision of solvent effects. *Chem. Phys.* **1981**, *55*, 117−129.

(18) Marenich, A. V.; Cramer, C. J.; Truhlar, D. G. Universal solvation model based on solute electron density and on a continuum model of the solvent defined by the bulk dielectric constant and atomic surface tensions. *J. Phys. Chem. B* **2009**, *113*, 6378−6396.

DOI: 10.1021/acs.accounts.6b00204
Acc. Chem. Res. 2016, 49, 1279−1291

(19) For a recent review, see: Flanigan, D. M.; Romanov-Michailidis, F.; White, N. A.; Rovis, T. Organocatalytic reactions enabled by *N*-heterocyclic carbenes. *Chem. Rev.* **2015**, *115*, 9307−9387.
(20) (a) Huerta, F. F.; Minidis, B. E.; Bäckvall, J.-E. Racemization in asymmetric synthesis. Dynamic kinetic resolution and related processes in enzyme and metal catalysis. *Chem. Soc. Rev.* **2001**, *30*, 321−331. (b) Caddick, S.; Jenkins, K. Dynamic kinetic resolutions in asymmetric synthesis. *Chem. Soc. Rev.* **1996**, *25*, 447−456.
(21) Tian, S.-K.; Chen, Y.; Hang, J.; Tang, L.; McDaid, P.; Deng, L. Asymmetric organic catalysis with modified cinchona alkaloids. *Acc. Chem. Res.* **2004**, *37*, 621−631.
(22) Cohen, D. T.; Eichman, C. C.; Phillips, E. M.; Zarefsky, E. R.; Scheidt, K. A. Catalytic dynamic kinetic resolutions with *N*-heterocyclic carbenes: asymmetric synthesis of highly substituted β-lactones. *Angew. Chem., Int. Ed.* **2012**, *51*, 7309−7313.
(23) Johnston, R. C.; Cohen, D. T.; Eichman, C. C.; Scheidt, K. A.; Cheong, P. H.-Y. Catalytic kinetic resolution of a dynamic racemate: highly stereoselective β-lactone formation by *N*-heterocyclic carbene catalysis. *Chem. Sci.* **2014**, *5*, 1974−1982.
(24) There is a possibility that the NHC is involved in the epimerization process. NMR experiments showed almost instant and complete deuterium incorporation at the α-positon of the β-keto ester. It is therefore postulated that the NHC acts only to catalyze stereospecific C−C bond formation.
(25) Addition of both Lewis acids and thiourea hydrogen-bond donors slowed or killed the reaction, in agreement with the reactive NHC−enolate model.
(26) Oh, S. H.; Cortez, G. S.; Romo, D. Asymmetric synthesis of bicyclic β-lactones via the intramolecular, nucleophile-catalyzed aldol lactonization: Improved efficiency and expanded scope. *J. Org. Chem.* **2005**, *70*, 2835−2838.
(27) Ryan, S. J.; Stasch, A.; Paddon-Row, M. N.; Lupton, D. W. Synthetic and quantum mechanical studies into the *N*-heterocyclic carbene catalyzed (4 + 2) cycloaddition. *J. Org. Chem.* **2012**, *77*, 1113−1124.
(28) All of the TSs were confirmed using intrinsic reaction coordinate (IRC) computations. For a recent review of the applications of IRC calculations, see: Maeda, S.; Harabuchi, Y.; Ono, Y.; Taketsugu, T.; Morokuma, K. Intrinsic reaction coordinate: Calculation, bifurcation, and automated search. *Int. J. Quantum Chem.* **2015**, *115*, 258−269.
(29) All distances are in angstroms, all dihedral angles in degrees, and all energies in kcal/mol. Figures were generated using CYLview: Legault, C. Y. *CYLview*, version 1.0b; Université de Sherbrooke: Quebec, Canada, 2009; http://www.cylview.org.
(30) Jang, K. P.; Hutson, G. E.; Johnston, R. C.; McCusker, E. O.; Cheong, P. H.-Y.; Scheidt, K. A. Asymmetric Homoenolate additions to acyl phosphonates through reational design of a tailored *N*-heterocyclic carbene catalyst. *J. Am. Chem. Soc.* **2014**, *136*, 76−79.
(31) Takenaka, N.; Abell, J. P.; Yamamoto, H. Asymmetric conjugate addition of silyl enol ethers catalyzed by tethered bis(8-quinolinolato) aluminum complexes. *J. Am. Chem. Soc.* **2007**, *129*, 742−743.
(32) Evans, D. A.; Scheidt, K. A.; Fandrick, K. R.; Lam, H. W.; Wu, J. Enantioselective indole Friedel-Crafts alkylations catalyzed by bis(oxazolinyl)pyridine-scandium triflate complexes. *J. Am. Chem. Soc.* **2003**, *125*, 10780−10781.
(33) Evans, D. A.; Johnson, J. S. Catalytic enantioselective hetero Diels-Alder reactions of α,β-unsaturated acyl phosphonates with enol ethers. *J. Am. Chem. Soc.* **1998**, *120*, 4895−4896.
(34) Gould, E.; Walden, D. M.; Kasten, K.; Johnston, R. C.; Wu, J.; Slawin, A. M. Z.; Mustard, T. J. L.; Johnston, B.; Davies, T.; Cheong, P. H.-Y.; Smith, A. D. Catalyst selective and regiodivergent *O*- to *C*- or *N*-carboxyl transfer of pyrazolyl carbonates: synthetic and computational studies. *Chem. Sci.* **2014**, *5*, 3651−3658.
(35) Höfle, G.; Steglich, W.; Vorbrüggen, H. 4-Diaklylamines as highly active acylation catalysts. *Angew. Chem., Int. Ed. Engl.* **1978**, *17*, 569−583.
(36) Ruble, J. C.; Fu, G. C. Enantioselective construction of quaternary stereocenters: rearrangements of *O*-acylated azlactones catalyzed by a planar-chiral derivative of 4-(pyrrolidino)pyridine. *J. Am. Chem. Soc.* **1998**, *120*, 11532−11533.
(37) Shaw, S. A.; Aleman, P.; Vedejs, E. Development of chiral nucleophilic pyridine catalysts: applications in asymmetric quaternary carbon synthesis. *J. Am. Chem. Soc.* **2003**, *125*, 13368−13369.
(38) Thomson, J. E.; Rix, K.; Smith, A. D. Efficient *N*-heterocyclic carbene-catalyzed *O*- to *C*-acyl transfer. *Org. Lett.* **2006**, *8*, 3785−3788.
(39) Mandai, H.; Fujiwara, T.; Noda, K.; Fujii, K.; Mitsudo, K.; Korenaga, T.; Suga, S. Enantioselective Steglich rearrangement of oxindole derivatives by easily accessible chiral *N*,*N*-4-(dimethylamino)-pyridine derivatives. *Org. Lett.* **2015**, *17*, 4436−4439.
(40) Hills, I. D.; Fu, G. C. Catalytic enantioselective synthesis of oxindoles and benzofuranones that bear a quaternary stereocenter. *Angew. Chem., Int. Ed.* **2003**, *42*, 3921−3924.
(41) (a) A stepwise DMAP-catalyzed C-carboxylation mechanism could not be located on the PES for the reaction. IRC calculations confirmed the concerted, asynchronous carboxylation of this particular pathway. (b) A similar concerted pathway was found in computations on DMAP-catalyzed acyl transfer to alcohols. See: Xu, S.; Held, I.; Kempf, B.; Mayr, H.; Steglich, W.; Zipse, H. The DMAP-catalyzed acetylation of alcohols−a mechanistic study (DMAP = 4-(dimethylamino)pyridine). *Chem. - Eur. J.* **2005**, *11*, 4751−4757.
(42) For a review of planar-chiral DMAP catalysis, see: Wurz, R. P. Chiral dialkylaminopyridine catalysts in asymmetric synthesis. *Chem. Rev.* **2007**, *107*, 5570−5595.
(43) For a recent review of ketene intermediates, see: Allen, A. D.; Tidwell, T. T. Ketenes and other cumulenes as reactive intermediates. *Chem. Rev.* **2013**, *113*, 7287−7342.
(44) Hodous, B. L.; Fu, G. C. Enantioselective addition of amines to ketenes catalyzed by a planar-chiral derivative of PPY: possible intervention of chiral Brønsted-acid catalysis. *J. Am. Chem. Soc.* **2002**, *124*, 10006−10007.
(45) Pattawong, O.; Mustard, T. J. L.; Johnston, R. C.; Cheong, P. H.-Y. Mechanism and stereocontrol: enantioselective addition of pyrrole to ketenes using planar-chiral organocatalysts. *Angew. Chem., Int. Ed.* **2013**, *52*, 1420−1423.
(46) (a) All k_H/k_D KIEs are reported using the Bigeleisen−Mayer approach for room temperature (25° C) and a scaling factor of 1.0. See: Bigeleisen, J.; Mayer, M. G. Calculation of equilibrium constants for isotopic exchange reactions. *J. Chem. Phys.* **1947**, *15*, 261−267. (b) The pyrrole−PPY* complex was the assumed resting state for all of the KIE computations.
(47) France, S.; Guerin, D. J.; Miller, S. J.; Lectka, T. Nucleophilic amines as catalysts in asymmetric synthesis. *Chem. Rev.* **2003**, *103*, 2985−3012.
(48) (a) Wang, B.; Tu, Y. Q. Stereoselective construction of quaternary carbon stereocenters via a semipinacol rearrangement strategy. *Acc. Chem. Res.* **2011**, *44*, 1207−1222. (b) Corey, E. J.; Guzman-Perez, A. The catalytic enantioselective construction of molecules with quaternary carbon stereocenters. *Angew. Chem., Int. Ed.* **1998**, *37*, 388−401. (c) Fuji, K. Aysmmetric creation of quaternary carbon centers. *Chem. Rev.* **1993**, *93*, 2037−2066.
(49) Pfau, M.; Revial, G.; Guingant, A.; d'Angelo, J. Enantioselective synthesis of quaternary carbon centers through Michael-type alkylation of chiral imines. *J. Am. Chem. Soc.* **1985**, *107*, 273−274.
(50) (a) Taylor, M. S.; Jacobsen, E. N. Asymmetric catalysis by chiral hydrogen-bond donors. *Angew. Chem., Int. Ed.* **2006**, *45*, 1520−1543. (b) Schreiner, P. R. Metal-free organocatalysis through explicit hydrogen bonding interactions. *Chem. Soc. Rev.* **2003**, *32*, 289−296.
(51) Kang, J. Y.; Carter, R. G. Primary amine, thiourea-based dual catalysis motif for synthesis of stereogenic, all-carbon quaternary center-containing cycloalkanones. *Org. Lett.* **2012**, *14*, 3178−3181.
(52) Kang, J. Y.; Johnston, R. C.; Snyder, K. M.; Cheong, P. H.-Y.; Carter, R. G. Construction of stereogenic α,α-disubstituted cycloalkanones via 1° amine thiourea dual catalysis: Experimental scope and computational analyses. *J. Org. Chem.* **2016**, *81*, 3629−3637.
(53) Experimental KIEs were determined at two separate reaction times. After 30 min, k_H/k_D = 0.82, and after 48 h, k_H/k_D = 0.86.

DOI: 10.1021/acs.accounts.6b00204
Acc. Chem. Res. 2016, 49, 1279−1291

(54) (a) Yalalov, D. A.; Tsogoeva, S. B.; Schmatz, S. Chiral thiourea-based bifunctional organocatalysts in the asymmetric nitro-Michael addition: A joint experimental-theoretical study. *Adv. Synth. Catal.* **2006**, *348*, 826−832. (b) Okino, T.; Hoashi, Y.; Takemoto, Y. Enantioselective Michael reaction of malonates to nitroolefins catalyzed by bifunctional organocatalysts. *J. Am. Chem. Soc.* **2003**, *125*, 12672−12673.
(55) For a recent review, see: Serdyuk, O. V.; Heckel, C. M.; Tsogoeva, S. B. Bifunctional primary amine-thioureas in asymmetric organocatalysis. *Org. Biomol. Chem.* **2013**, *11*, 7051−7071.
(56) Hajos, Z. G.; Parrish, D. R. Asymmetric synthesis of bicyclic intermediates of natural product chemistry. *J. Org. Chem.* **1974**, *39*, 1615−1621.
(57) (a) Notz, W.; Tanaka, F.; Barbas, C. F., III Enamine-based organocatalysis with proline and diamines: The development of direct catalytic asymmetric aldol, Mannich, Michael, and Diels-Alder reactions. *Acc. Chem. Res.* **2004**, *37*, 580−591. (b) List, B. Proline-catalyzed asymmetric reactions. *Tetrahedron* **2002**, *58*, 5573−5590.
(58) (a) Zhu, H.; Clemente, F. R.; Houk, K. N.; Meyer, M. P. Rate limiting step precedes C-C bond formation in the archetypical proline-catalyzed intramolecular aldol reaction. *J. Am. Chem. Soc.* **2009**, *131*, 1632−1633. (b) Zotova, N.; Franzke, A.; Armstrong, A.; Blackmond, D. G. Clarification of the role of water in proline-mediated aldol reactions. *J. Am. Chem. Soc.* **2007**, *129*, 15100−15101.
(59) (a) Allemann, C.; Gordillo, R.; Clemente, F. R.; Cheong, P. H.-Y.; Houk, K. N. Theory of asymmetric organocatalysis of aldol and related reactions: Rationalizations and predictions. *Acc. Chem. Res.* **2004**, *37*, 558−569. (b) Clemente, F. R.; Houk, K. N. Computational evidence for the enamine mechanism of intramolecular aldol reactions catalyzed by proline. *Angew. Chem., Int. Ed.* **2004**, *43*, 5766−5768. (c) Bahmanyar, S.; Houk, K. N. The origin of stereoselectivity in proline-catalyzed intramolecular aldol reactions. *J. Am. Chem. Soc.* **2001**, *123*, 12911−12912.
(60) For the original experimental article by Carter, see: Yang, H.; Carter, R. G. Synthesis of all-carbon, quaternary center-containing cyclohexenones through an organocatalyzed, multicomponent coupling. *Org. Lett.* **2010**, *12*, 3108−3111. For our computational investigation, see: Pierce, M. D.; Johnston, R. C.; Mahapatra, S.; Yang, H.; Carter, R. G.; Cheong, P. H.-Y. Mechanism and stereoselectivity of a dual amino-catalyzed Robinson annulation: Rare duumvirate stereocontrol. *J. Am. Chem. Soc.* **2012**, *134*, 13624−13631.
(61) There appears to be confusion regarding the official pronunciation of this term. It is pronounced as “du-um-virate”, as opposed to “dumb-virate”.

DOI: 10.1021/acs.accounts.6b00204
Acc. Chem. Res. 2016, 49, 1279−1291